Wall forces produced during ITER disruptions

H.R. Strauss[1], R. Paccagnella[2], J. Breslau[3]
[1]HRS Fusion, West Orange NJ, USA 07052
[2] Consorzio RFX and Istituto Gas Ionizzati (C.N.R), Padua, Italy
[3] Princeton Plasma Physics Laboratory, Princeton, NJ 08570
strauss@cims.nyu.edu

Abstract

Nonlinear simulations with the M3D [1] code are performed of disruptions produced by large scale magnetohydrodynamic (MHD) instabilities. The toroidally symmetric and asymmetric wall forces produced during a disruption are calculated in an ITER model. The disruption is produced by a vertical displacement event (VDE) and a kink mode. Expressions are derived for the wall force, including the sideways force, using a thin conducting wall model. The scaling of wall force with plasma current and $\gamma\tau_w$ is obtained, where γ is the kink growth rate and τ_w is the wall penetration time. The worst case is with $\gamma\tau_w \approx 1$. A theory is developed of the wall force produced by kink modes. The theory is in qualitative agreement with the simulations and JET experiments. In particular, the theory and simulations give correlations of sideways force with sideways plasma displacement, and of toroidally varying plasma current with toroidally varying vertical displacement.

I. Introduction

A very critical issue for the ITER device construction is to evaluate the forces produced on the surrounding conducting structures during plasma disruptions [2]. Recent studies have documented results obtained from the JET experiment [3, 4, 5]. A major concern are non axisymmetric stresses caused by large scale MHD instabilities [6]. We extend previous studies of vertical displacement events combined with disruptions [7]. In particular, in this paper the emphasis is on the non axisymmetric wall forces. New numerical diagnostics are derived and implemented, which directly measure the forces in the resistive shell surrounding the plasma. The disruptions are simulated using the M3D [1] code. The code solves resistive MHD equations with parallel and perpendicular thermal transport. The plasma is bounded by a thin, resistive wall [8] of thickness δ. The magnetic field perturbations outside the wall are calculated with Green's functions [9, 10]. The jump in the magnetic field across the thin wall gives the wall force.

Numerical studies of disruptions at first used helical symmetry [11]. In the case of zero magnetic shear, the plasma could deform into large magnetic bubbles. In the presence of magnetic shear, the bubbles were suppressed. Three dimensional reduced MHD [12] simulations [13] showed that overlap of magnetic islands produced a chaotic rupturing of the magnetic field and loss of equilibrium. The magnetic field chaos causes quenching of the plasma current and pressure.

The forces and stresses on the wall are due to currents flowing in the wall that couple with the magnetic field. These currents are produced by inductive effects (eddy

currents), due to time varying magnetic fluxes through the wall and also by conduction currents, generally indicated as halo currents, that can flow from the plasma to the wall. In the first case the plasma acts as a voltage generator and the wall current adjusts according to the wall conductivity, while in the second case, the plasma is a current generator and the current penetrating the wall is mainly determined by the MHD evolution inside the plasma and in the outside region next to the wall. In this case also, the wall resistivity affects the current, but in a more indirect way, through the effect on the MHD instabilities of the resistive wall boundary conditions.

The present simulations are based on an ITER reference equilibrium. Disruptions were produced by an axi-symmetric vertical displacement event (VDE), along with a large scale kink instability. This is expected to be one of the worst case scenarios. The scaling of the asymmetric wall force with current and wall penetration time was investigated. The wall force is proportional to the growth rate of the instability multiplied by the square of the current. For very large current and growth rate, it appears to saturate. This behavior has a simple explanation, since increasing the current (for a given toroidal magnetic field) is equivalent in our model to decreasing the values of the safety factor, q, in the plasma and in particular decreasing the on axis q below 1. This triggers fast kink modes. Looking at the effect of the wall penetration time for these instabilities, we have found that the wall force increases in the regime $\gamma\tau_w \sim 1$. This is obtained in the simulations, for a given current profile, by reducing the wall conductivity. This behavior indicates that the force at the wall, *i.e.* the total current flowing in the wall due to induction and conduction effects, is affected by the wall conductivity in such a way that the worst case scenario happens when a substantial flux penetration through the wall is allowed.

Beside numerical results, a theory of wall force is developed, which is in qualitative agreement with the simulations. The theory agrees with the scaling of wall force with plasma current. The theory and simulations give correlations of sideways force with sideways plasma displacement, and of toroidally varying plasma current with toroidally varying vertical displacement. The correlations of force and plasma displacement are positive, until the plasma current touches the wall. A net toroidal variation of of the plasma current is produced in the presence of a VDE and a kink mode, even when the plasma current is not in contact with the wall. The positive correlation of plasma current variation with plasma displacement does not establish the Hiro current theory of wall force [6]. The paper is organized as follows. The resistive wall model, including the derivation of the wall force, halo current, and toroidal peaking factor (TPF), is described in section II. In section III the disruption simulations are presented, beginning with a brief description of the numerical method. Simulational results are presented, including scaling of the wall force with plasma current, halo current, and TPF. Analysis of the wall force with a circular cross section, constant current model, is presented in section IV. Conclusions are presented in section V.

II. Resistive Wall Model

The plasma (or blanket) is bounded by a thin resistive wall. Surrounding this is an outer vacuum region, which can contain external current sources.

The vacuum field is represented as [8]

$$\mathbf{B}_v = \nabla\psi^v \times \nabla\phi + \nabla\lambda + R_0 B_0 \nabla\phi \tag{1}$$

where B_0 is the toroidal magnetic field on axis. The reason for this term, as well as ψ^v, is to be able to match the vacuum solution to a plasma equilibrium with a net current, and net toroidal magnetic field, using a single valued function λ of poloidal and toroidal angle. The function ψ^v depends on the poloidal coordinates R, Z and is independent of toroidal angle ϕ. It satisfies the vacuum Grad Shafranov equation $\Delta^*\psi^v = R^2\nabla R^{-2} \cdot \nabla\psi^v = 0$.

To satisfy $\nabla \cdot \mathbf{B}_v = 0$, $\nabla^2\lambda = 0$. On the resistive wall boundary, integrating $\nabla \cdot \mathbf{B}$ across the thin shell gives the requirement that the normal component of magnetic field is continuous at the wall,

$$B_n^v = B_n^p,$$

where B_n^v, B_n^p are the normal component of magnetic field in the vacuum, just outside the wall, and the plasma (or blanket), just inside the wall. This gives a boundary condition to determine the vacuum field.

The vacuum field is solved by the GRIN code [9]. From Green's identity one has an integral equation relating $\partial\psi^v/\partial n$ to given ψ^v, and λ_n to given $\partial\lambda_n/\partial n$ on the boundary contour [10] When discretized, these integral equations become matrix equations which are set up and solved by GRIN. Given a set of boundary points, R_i, Z_i,

$$(\frac{\partial\psi^v}{\partial n})_i = \sum_j K_{ij}^0 \psi_j^p + S_{xi}, \tag{2}$$

$$\lambda_i^n = \sum_j K_{ij}^n (B_n^p)_j \tag{3}$$

where K_{ij}^0, K_{ij}^n are matrices that can be precomputed given the set of boundary points. The external source term S_x in (3) can be obtained from the applied external currents, or else using the "virtual casing" method. The source term S_x is chosen so that at the initial time, $\partial\psi^v/\partial n = \partial\psi^p/\partial n$.

Now the magnetic field components in the plasma have to be matched at the thin resistive shell of thickness δ and resistivity η_w. The boundary conditions are

$$\hat{\mathbf{n}} \times (\mathbf{E}^v - \mathbf{E}^p) = 0$$

where $\mathbf{E} = \eta_w \mathbf{J}$ and $\hat{\mathbf{n}}$ is the outward normal to the wall. In the wall, the current is given by,

$$\mathbf{J} = \frac{1}{\mu_0 \delta} \hat{\mathbf{n}} \times (\mathbf{B}^v - \mathbf{B}^p). \tag{4}$$

The normal component of the magnetic field is continuous at the wall: it satisfies

$$\frac{\partial B_n}{\partial t} = -\frac{\eta_w}{\delta}\nabla \cdot [\hat{\mathbf{n}} \times (\mathbf{B}^v - \mathbf{B}^p) \times \hat{\mathbf{n}}] \tag{5}$$

The normal component of the wall force density is

$$f_{wn} = \hat{\mathbf{n}} \cdot \mathbf{J}_w \times \mathbf{B}_w.$$

Inside the wall assume that

$$\mathbf{B}_w = \frac{1}{2}(\mathbf{B}^v + \mathbf{B}^p).$$

The normal wall force density can be expressed

$$f_{wn} = \frac{1}{2\mu_0\delta}(|\mathbf{B}^p|^2 - |\mathbf{B}^v|^2). \tag{6}$$

It has a simple physical meaning. It is the difference in magnetic pressure across the wall, divided by the wall thickness. Integrating over the wall thickness δ gives the magnetic pressure on the wall.

The tangential components of the wall force multiplied by the wall thickness are

$$f_{wl} = J_\phi B_n = \frac{B_n}{\mu_0\delta}(B_l^v - B_l^p), \tag{7}$$

$$f_{w\phi} = -J_l B_n = \frac{B_n}{\mu_0\delta}(B_\phi^v - B_\phi^p), \tag{8}$$

where $\hat{\mathbf{l}} = -\hat{\mathbf{n}} \times \hat{\phi}$.

The total wall force per toroidal angle is given by

$$\mathbf{F} = \frac{\mu_0\delta}{2\pi R_0 L_w B_0^2}\int dl R(f_{wn}\hat{\mathbf{n}} + f_{wl}\hat{\mathbf{l}} + f_{w\phi}\hat{\phi}). \tag{9}$$

Here the force has been normalized to be dimensionless, where B_0 is the magnetic field on axis, and $L_w = \int dl$ is the wall circumference. To obtain the dimensional force, (9) must be multiplied by $F_{dim} = 2\pi R_0 L_w B_0^2/\mu_0$. Of particular importance is the net horizontal force, F_x. Here F_x is obtained by taking the horizontal components of $\mathbf{F}$, $F_c = \int d\phi \mathbf{F} \cdot \hat{\mathbf{R}} \cos(\phi)$, $F_s = \int d\phi \mathbf{F} \cdot \hat{\mathbf{R}} \sin(\phi)$. To allow for the horizontal force to be an arbitrary direction, the horizontal force is

$$F_x = (F_c^2 + F_s^2)^{1/2}.$$

It is in units of F_{dim}.

The wall force is produced by induced wall current, as well as by halo currents, which are poloidal currents penetrating the wall, parameterized by the halo current fraction F_{halo} of the total current. The asymmetry of the halo current, parameterized

by the toroidal peaking factor (TPF), is also important for calculation of stress on conducting structures. Nonlinear simulations of VDEs, disruptions, and resistive wall modes with the M3D code [1] found F_{halo} and TPF consistent with experimental data [14, 7].

The halo current is the poloidal current flowing into the resistive wall. The normal component of the poloidal current integrated over the wall, I_{halo}, is

$$I_{halo}(\phi) = \frac{1}{2}\int |\hat{n}\cdot\mathbf{J}|Rdl,$$

where dl is the length element tangent to the wall. Half the absolute value is taken in the integrand because $\nabla\cdot\mathbf{J}=0$ implies the total normal current is zero when integrated over the wall and the toroidal angle ϕ. The toroidal peaking factor [15] is defined as the maximum of

$$\mathrm{TPF} = \frac{2\pi \mathrm{I_{halo(max)}}}{\int \mathrm{I_{halo}} \mathrm{d}\phi}.$$

In the following simulations, TPF ≈ 2. The ratio of halo current to total plasma current is also important. The halo current fraction F_{halo} is defined as the ratio

$$F_{halo} = \frac{\int I_{halo} d\phi}{\int I_\phi d\phi},$$

where the toroidal current is $I_\phi = \int J_\phi dRdZ$.

The tangential wall current is related to the halo current. The tangential wall current is

$$J_l = \frac{1}{\mu_0\delta}(B_\phi^v - B_\phi^p). \tag{10}$$

But $\mu_0 J_n = (1/R)\partial(RB_\phi^p)/\partial l - (1/R)\partial(B_l^p)/\partial\phi$, so that

$$RB_\phi^p = \mu_0 \int^l dl'(RJ_n + \frac{\partial B_l^p}{\partial\phi})$$

where the first integral on the right is related to the halo current. Hence the terms, $J_l B_\phi$, which is part of the normal wall force (6), and $J_l B_n$, which gives the toroidal wall force (8), are related to the halo current.

III. Disruption Simulation

The M3D extended MHD code [1] solves the full resistive MHD equations. The open field line region surrounding the plasma is treated as a resistive MHD vacuum with very large resistivity, small density, and low temperature. A resistive wall with the shape of the experimental vacuum vessel, slightly smoothed, bounds the vacuum. The code does not assume large aspect ratio or incompressibility and it keeps the full plasma X-point geometry. The plasma velocity is evolved self-consistently, by solving the MHD momentum evolution equations. Advection terms are treated numerically with an upwind advection method [16]. It was also very helpful to use dealiasing [17] in the toroidal direction, eliminating the upper third of the toroidal mode spectrum.

Upwinding and dealiasing provided adequate numerical stabilization to permit the simulation of complete disruption events.

A single, scalar temperature is assumed, with the ion and electron temperatures taken to be proportional. Temperature evolution includes parallel[18] and perpendicular thermal transport. The effective parallel thermal diffusion coefficient is $\kappa_\parallel = 2Rv_A$, much larger than the perpendicular diffusion, where R is the major radius and v_A is the Alfvén speed. The resistivity varies as $T^{-3/2}$ self-consistently, where T is the temperature. Spatially constant perpendicular thermal conductivity $\kappa_\perp$ and viscosity $\mu_\perp$ were employed.

M3D uses an unstructured mesh [19] with a finite element discretization in the poloidal, (R, Z) plane. In the toroidal direction, a uniform mesh in toroidal angle ϕ is used, with a pseudospectral discretization. The mesh boundary is treated as a thin resistive wall. Outside the resistive wall is the vacuum region.

In the following, M3D is used to calculate a disruption. The initial state is an ITER reference equilibrium, FEAT15MA, written to a file in EQDSK [20] format. This was read into M3D and used to generate a mesh and initialize a nonlinear simulation. The initial equilibrium had $q = 1.1$ on axis.

In the simulation the Lundquist number was chosen to be $S = 10^5$ on axis and $S = 10^2$ at the wall. The Lundquist number must be much lower than experiment for numerical reasons. The resistivity is calculated self consistently as $T^{-3/2}$, where T is the temperature. When the temperature decays during the simulation, the value of S drops, although its value is held fixed at the wall. The wall resistivity η_w divided by wall thickness, was chosen to have a range of values. In the following example of Fig.1, $\tau_w v_A/R = 10^2$. The perpendicular thermal diffusivity was $\kappa_\perp = 10^{-5}\epsilon a v_A$, and the viscous diffusivity was $\mu_\perp = 10^{-4}\epsilon a v_A$, where a is the effective minor radius and $\epsilon = a/R$.

The velocity boundary condition was $v_n = 0$. The magnetic field boundary condition was given by (5).

The initial equilibrium is VDE unstable. The equilibrium was made to be kink unstable by rescaling. The initial equilibrium had $q_0 = 1.1$, and initial total current I_0. The equilibrium was rescaled to generate equilibria with $q < 1$ on axis, and $1 < I/I_0$. The poloidal magnetic field and toroidal current were rescaled by multiplying by a rescaling parameter, and the pressure was rescaled by the square of the rescaling parameter. Such a state might be produced during a VDE, as current is scraped off by a wall interaction.

The following example was produced by first evolving a VDE, then adding a kink perturbation as the plasma approached the wall. Fig.1 shows the nonlinear kink and VDE at time $t = 40.9\tau_A$ after adding the kink perturbation. The wall resistivity for this example had $\gamma\tau_w \approx 15$, and the current enhancement was $I/I_0 = 1.6$. The poloidal magnetic flux is shown in Fig.1(a), and the toroidal current density $C = -RJ_\phi$ in Fig.1(b). A current sheet is visible on the side of the current next to the wall. The temperature T is shown in Fig.1(c). The contours are all shown in the poloidal plane

(R, Z) with toroidal angle $\phi = 0$.

In Fig.2, at time $t = 51\tau_A$, the plasma is contact with the wall. Fig.2(a) shows the poloidal magnetic flux penetrating the wall. Fig.2(b) shows the current. The sheet current now has a dipole structure. This is because the current distribution in the plasma is not uniform, but is peaked on axis. The displacement inside the plasma pushes the current peak to the edge of the plasma, where it forms a dipole structure with the skin current. The temperature in Fig.2(c) is also peaked near the wall, similarly to the current, Both the current dipole and the temperature peak have a helical structure. A short time later, $t = 54.3\tau_A$, shown in Fig.3, both the current dipole and the temperature peak are disappear from the plasma.

The distribution of the normal wall force density, $f_n(\theta, \phi)$, is shown in Fig.4 at time $t = 51\tau_A$. The horizontal coordinate θ is the poloidal angle of the wall from the origin $(R, Z) = (R_0, 0)$, starting at the outboard midplane, going counter clockwise. The vertical axis is the toroidal angle ϕ. The force structure is concentrated at the top of the wall. $\theta \approx \pi/2$, and has an $(m, n) = (1, 1)$ structure.

The time history of the normalized total pressure, total toroidal current, halo current fraction and TPF are shown in Fig.5(a). The current is normalized to I_0. The pressure is in units of β, multiplied by 30 to fit on the same graph as the current. The TPF peaks first, at about 2.4 Next the pressure quench begins, followed by the current. The halo current fraction F_{halo} peaks during the current quench.

The averaged horizontal wall force F_x is shown in Fig.5(b). It peaks during the current quench.

In terms of ITER parameters, the toroidal field is $B_\phi = 5.3T$, producing a magnetic pressure of $2.24 \times 10^7 N/m^2$. Multiplying by the plasma surface area $2\pi \int dl R = 804\text{m}^2$ gives the total wall force in ITER $F_{dim}^{ITER} = 1.81 \times 10^{10} N$. The horizontal wall force is $F_x \times F_{dim}$. In ITER terms, the peak sideways force in Fig.5(b) is $F_x^{ITER} = F_x \times F_{dim}^{ITER} = 65MN$. This is about the predicted value used in the ITER design. The total wall force F_{dim} scales as I_p^2, where $I_p \propto Ba$ is the plasma current, assuming fixed aspect ratio and q. The ITER current is about 5 times greater than the JET current, so that the JET horizontal force could be as large as 2.75 MN. This value is consistent with experiments.

A scaling study the sideways force was performed by comparing results obtained with different I/I_0. A sequence of equilibria was produced by rescaling. In these cases, the VDE was not evolved first. The scaling of the horizontal, sideways force, is shown in Fig.6. The data can be fit with a quadratic scaling, $F_x \propto \gamma\tau_A (I/I_0)^2$, where γ is the maximum mode growth rate, and $\tau_A = R/v_A$ is the toroidal Alfvén transit time. This scaling is consistent with the theory derived below. It fits for for smaller I/I_0, but it saturates for larger I/I_0. It is similar to a scaling reported for VDEs [4].

The scaling of wall force with wall resistivity was obtained for equilibria with $I/I_0 = 1.6$, varying τ_w. This was also without a VDE. The results are shown in Fig.7. The results are insensitive to the wall penetration time in the regime $\gamma\tau_w \to \infty$. In this regime the wall is a good conductor, and induced wall current produces the wall

force. In the case $\gamma\tau_w \sim 1$, there is significant magnetic flux penetration through the wall, and the wall force is somewhat larger. In this case apparently there is a competition between the kink amplitude increase and stochasticity produced in the plasma. When the wall is a good conductor, the current interacts with the wall and the kink reaches a relatively high amplitude before stochasticity fully develops and smooths out the kink perturbation and plasma current. In the "insulating" limit $\gamma\tau_w \to 0$, the magnetic field is continuous and the force should eventually vanish.

IV. Analytic model of wall force

The wall force dependence on current and wall resistivity can be estimated using a simple analytic model. The magnetic field is approximately,

$$\mathbf{B} = \nabla\psi \times \hat{\phi} + B\hat{\phi}, \tag{11}$$

assuming a simple circular flux surface geometry (r, θ, ϕ). Assume constant toroidal current $-j_\phi = \nabla^2\psi_0 = 2B/q_0R_0$ inside the plasma boundary at $r = a$. Then $B_\theta = -Br/(qR)$ for $r \le a$. The linearized equations describing the plasma [12] are

$$\psi = \mathbf{B}_0 \cdot \nabla\Phi \tag{12}$$

$$\gamma^2\nabla \cdot \rho\nabla\Phi = \mathbf{B}_0 \cdot \nabla\nabla^2\psi_1 + \mathbf{B}_1 \cdot \nabla\nabla^2\psi_0 \tag{13}$$

where $\rho = 0, r > a$, and $\rho = 1, r \le a$. The plasma displacement ξ is

$$\xi = \nabla\Phi \times \hat{\phi}. \tag{14}$$

The perturbations are proportional to $\exp(i\alpha)$, where $\alpha = m\theta + n\phi$, and $B \cdot \nabla \exp(i\alpha) = iBk_\parallel \exp(i\alpha)$, where $k_\parallel = (qR)^{-1}(-m + nq)$. Integrating (13) across the plasma - vacuum interface and using (12) to eliminate Φ, gives

$$(\frac{\gamma}{v_A})^2 \frac{1}{k_\parallel}\psi_p' = k_\parallel(\psi_v' - \psi_p') - \frac{2m}{aqR}\psi_p \tag{15}$$

In the plasma region, $r \le a$, the magnetic perturbation is

$$\psi_p = \psi_{1\alpha}(r/a)^m \exp(i\alpha), \tag{16}$$

and in the vacuum region $a < r \le b$,

$$\psi_v = [\psi_{2\alpha}(r/a)^m + \psi_{3\alpha}(a/r)^m] \exp(i\alpha). \tag{17}$$

Equate $\psi_p = \psi_v$ at $r = a$. Outside the resistive wall, $r > b$, the magnetic perturbation in the exterior vacuum region is

$$\psi_x = \psi_{4\alpha}(b/r)^m \exp(i\alpha). \tag{18}$$

Continuity at the resistive wall gives $\psi_x = \psi_v$ at $r = b$. At the wall, (5) is

$$\gamma\psi_x = \frac{\eta_w}{\delta}(\psi_x' - \psi_v') \tag{19}$$

which yields

$$(\gamma + \frac{\eta_w m}{\delta b})\psi_{4\alpha} = -\frac{\eta_w}{\delta}\psi_v'$$

Using this expression and continuity at $r = a$ and $r = b$, it is possible to express $\psi_{2\alpha}, \psi_{3\alpha}, \psi_{4\alpha}$ in terms of $\psi_{1\alpha}$. The skin current integrated across the jump at $r = a$ is

$$K_a = -\int dr \nabla^2 \psi = \psi_p' - \psi_v' \tag{20}$$

Similarly, the integrated skin current induced on the wall at $r = b$ is

$$K_b = \psi_v' - \psi_x' \tag{21}$$

Using expressions for $\psi_{2\alpha}, \psi_{3\alpha}, \psi_{4\alpha}$ in terms of $\psi_{1\alpha}$, (20),(21) give

$$K_a = 2\frac{m}{a}\frac{1 + 2/(\gamma\tau_w)}{1 - (a/b)^{2m} + 2/(\gamma\tau_w)}\psi_{1\alpha} \tag{22}$$

$$K_b = -2\frac{m}{b}\frac{(a/b)^m}{1 - (a/b)^{2m} + 2/(\gamma\tau_w)}\psi_{1\alpha} \tag{23}$$

where here $\tau_w = \delta b/(m\eta_w)$. The relations for $\psi_{2\alpha}, \psi_{3\alpha}, \psi_{4\alpha}$ can also be substituted into (15) to yield the dispersion relation,

$$\frac{1}{2}[1 - (\frac{a}{b})^{2m}](\frac{\gamma}{v_A})^2 = -\frac{1 + 2/(\gamma\tau_w)}{1 - (a/b)^{2m} + 2/(\gamma\tau_w)}k_\parallel^2 - \frac{k_\parallel}{Rq} \tag{24}$$

In the limit $\eta_w \to 0$, the kink mode is unstable for

$$m - 1 + (\frac{a}{b})^{2m} < nq < m \tag{25}$$

In the opposite limit, $\eta_w \to \infty$, the kink mode is unstable for

$$m - 1 < nq < m \tag{26}$$

This is reasonable, because with an ideally conducting wall, there is wall stabilization, while with an insulating wall, there is no wall stabilization.

The normal force density acting on the wall is

$$f_r = -\frac{B_\theta}{\delta}K_b \tag{27}$$

The magnetic perturbation $\psi_{1\alpha}$ is expressed in terms of the plasma displacement ξ_r using (11),(14). It is given by

$$\psi_{1\alpha} = \frac{a}{m}k_\parallel \xi_{r\alpha} \tag{28}$$

Hence

$$f_r = 2\frac{B_\theta^2}{\delta}\frac{(m - nq)(a/b)^m}{1 - (a/b)^{2m} + 2/(\gamma\tau_w)}\xi_{r\alpha} \tag{29}$$

This gives an approximately γB_θ^2 or $\gamma I^2/I_0^2$ scaling, taking for small growth rate, $\gamma \propto (m-nq)$. The force in the radial direction $\hat{\mathbf{R}}$ can be obtained by using (28),(29), noting that $\xi_R = \cos\theta\xi_r$, and integrating

$$F_R = -\frac{B_\theta}{2\pi}\int d\theta \cos\theta K_b$$

to obtain, if $m = n = 1$,

$$F_R = B_\theta^2 \frac{(1-q)(a/b)}{1-(a/b)^2+2/(\gamma\tau_w)}\xi_{R.} \tag{30}$$

Intuitively, this is reasonable: the displacement ξ_R causes magnetic field to be compressed at the wall. The vertical displacement, from (14) is related to the horizontal displacement. Taking $\psi = \psi_1(r/a)\cos(\theta+\phi)$, then $\Phi = \Phi_1(r/a)\sin(\theta+\phi)$. This can be expressed as $\Phi = (\Phi_1/a)(Z\cos\phi+(R-R_0)\sin\phi)$, so that $\xi_R = \partial\Phi/\partial Z = (\Phi_1/a)\cos\phi$ and $\xi_Z = -\partial\Phi/\partial Z = -(\Phi_1/a)\sin\phi$. Hence

$$\partial\xi_Z/\partial\phi = -\xi_R. \tag{31}$$

In the above, the signs of $j_{\phi 0}/B, B_\theta/B$ are negative, and $\psi_1 \propto \exp(im\theta + in\phi)$. It can be verified that the same results hold if signs of $j_{\phi 0}/B, B_\theta/B$ are positive, and $\psi_1 \propto \exp(im\theta - in\phi)$.

The vertical force can be obtained by using (28),(29), noting that $\xi_Z = \sin\theta\xi_r$, and integrating

$$F_Z = -\frac{B_\theta}{2\pi}\int d\theta \sin\theta K_b$$

to obtain, if $m = n = 1$,

$$F_Z = B_\theta^2 \frac{(1-q)(a/b)}{1-(a/b)^2+2/(\gamma\tau_w)}\xi_Z. \tag{32}$$

According to (30), (32), F_R, F_Z have the same sign as ξ_R, ξ_Z. From (22),(23) the skin current in the plasma has the opposite sign as the induced wall current. If the wall force is produced by transfer of the plasma skin current to the wall [6], then F_R, F_Z will have the sign of $-\xi_R, -\xi_Z$. This correlation can be compared with experiment.

In JET [6], the quantity $dI_\phi/d\phi$ was measured, where I_ϕ is the toroidal plasma current as a function of toroidal angle, and was compared to the ϕ derivative of the vertical plasma displacement $d\xi_Z/d\phi$. The current was measured in disruptions in which there was usually an upward VDE, and occasionally a downward VDE. This implies that the perturbations are shifted by the VDE displacement,

$$J_\phi = J_{\phi 0}(r - \xi_{vde}\sin\theta) + J_{\phi 1}(r-\xi_{vde}\sin\theta)\cos(\theta+\phi) \tag{33}$$

where $\xi_{vde} > 0$ for an upward displacement. The vertical VDE displacement ξ_{vde} interacts with the helical kink. Effectively the ξ_{vde} displacement gives a $\sin\theta$ weighting of the current. The total toroidally varying plasma current is

$$I_\phi = -\int drrd\theta \frac{dJ_{\phi 1}}{dr}\xi_{vde}\sin\theta\cos(\theta+\phi) = -\pi\xi_{vde}\int dr J_{\phi 1}\sin\phi.$$

where $J_{\phi 1}$ was first Taylor expanded and then integrated by parts. The quantity M_{IZ} is also measured in experiments. It is the vertical moment of the plasma current,

$$M_{IZ} = \int d\theta dr r^2 \sin\theta J_{\phi 1} \cos(\theta + \phi) = -\pi \int dr r^2 J_{\phi 1} \sin\phi.$$

Using $J_{\phi 1} = K_a \delta(r - a)$, yields

$$\frac{dI_\phi}{d\phi} = \frac{\xi_{vde}}{a^2} \frac{dM_{IZ}}{d\phi} \tag{34}$$

Using (20), M_{IZ} can be expressed as

$$M_{IZ} = I_\phi (1 - q) \xi_Z. \tag{35}$$

In JET experiments, $dI_\phi/d\phi$ and $dM_{Iz}/d\phi$ were found to be perfectly correlated with the sign of the VDE, or ξ_{vde}, as in (34). The net toroidal variation of I_ϕ is here not caused by current flowing into the wall [6], but by the vertical asymmetry produced by the VDE displacement.

The correlations were checked in simulations. Fig.8 shows time history of $FX = C(F_R, \xi_R)$, $FY = C(F_Z, \xi_Z)$, $XY = C(\xi_R, d\xi_Z/d\phi)$, and $CY = C(I_\phi, M_{IZ})$, for $I/I_0 = 2.0$, where

$$C(a, b) = \frac{(\int d\phi ab)}{(\int d\phi a^2)^{1/2} (\int d\phi b^2)^{1/2}}.$$

Until the current touches the wall, the correlations agree with (30),(31),(32). At that point, the sign of the wall force changes. The correlation CY is less good, with (34), but is positive. The correlation CY between I_ϕ and M_{IZ} holds even before the current contacts the wall. The correlations FX,FY show that the force $\mathbf{F} \propto \xi$ with a positive sign, until the current reaches the wall. The XY correlation shows that $\xi_R \approx -d\xi_Z/d\phi$.

The circular model equilibrium used here omits both the shear of the plasma current and the cross section shape, both of which should have a significant effect on the wall force. However we do not expect that these features change the qualitative results.

V. Discussion and conclusion

The toroidally symmetric and asymmetric wall forces produced during a disruption are calculated in an ITER model. A new method is derived for calculating wall forces directly from magnetic field pressure at a resistive wall. Simulations were done with M3D using an ITER reference equilibrium, modified so that it was both VDE and kink unstable. An example was chosen in which a VDE carried the plasma close to the wall, when it became kink unstable. The simulations show that the pressure, current and wall force are quenched by the contact of the plasma with the wall. We remark that the VDE kink simulation that we have presented so far is not fully self-consistent. In fact, the plasma edge should be scraped off or cooled by the plasma wall

interaction. This should cause the current channel to shrink, and the current density to increase, so that q on axis will decrease in time. This will in turn enhance plasma instability and trigger the kink mode. In the simulation presented here, the current is rescaled initially. A completely self consistent treatment will require additional physics modeling of the plasma wall interaction.

A study was carried out of the scaling of the asymmetric wall force with growth rate and current. The horizontal force is proportional to the growth rate of the instability multiplied by the square of the current, then saturates at high current, as shown in Fig.6.

The dependence of wall force on wall resistivity was also studied. If the wall is a relatively good conductor, such that $\gamma\tau_w \gg 1$, the wall resistivity has little effect. In the case, $\gamma\tau_w \approx 1$, the wall force is somewhat larger. We interpret this as the result of a competition between the growth of the kink, which affects both halo and eddy currents, and the plasma magnetic field stochastization, which smooths out plasma pressure and current gradients, reducing the level of plasma instability, and therefore slowing down the kink.

On the other hand, the insulating wall rapidly dissipates the wall current. In the limit $\gamma\tau_w \rightarrow 0$, the wall can not carry any current, and the wall force must vanish. Halo currents also remain small.

A theory is developed of the wall force produced by kink modes. The theory is in qualitative agreement with the simulations. In particular, the theory and simulations give positive correlation of sideways force with sideways plasma displacement, and the asymmetric vertical force with vertical plasma displacement. A net toroidal variation of of the plasma current is produced in the presence of a VDE, whether the plasma contacts the wall or not. In the case of an upward VDE interacting with a kink mode, toroidal variation of plasma current is positively correlated to the toroidal variation of the vertical component of the kink displacement.

In conclusion, in this paper we have presented a self consistent model of 3D MHD disruption simulations. Within this model we calculated the wall forces, with particular emphasis on the non axi-symmetric sideways force. We found for ITER a force in the range of 65 MN, a value somewhat larger but near to that used to design the machine. In future work, we plan to compare simulation results with experimental data from JET, NSTX, and other tokamaks. We also plan to generalize the wall model to study the effects of both a first wall and outer vacuum shell, which are planned for ITER.

Acknowledgments

This work was supported in part (H.S. and J.B.) by the U.S.D.O.E and in part (R.P.) by EFDA.

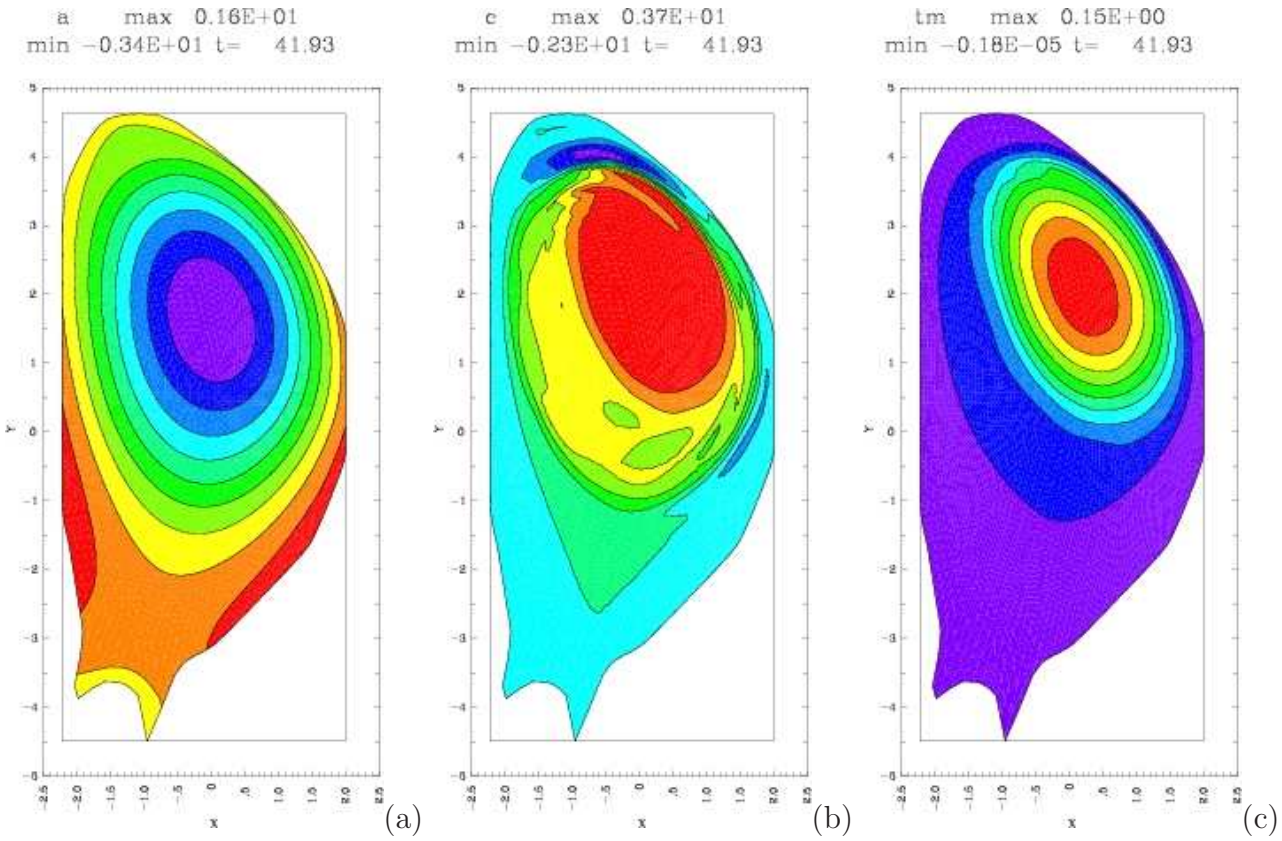

Figure 1: (a) poloidal flux ψ, (b) toroidal current $-RJ_\phi$, (c) temperature T, at $t = 40.9\tau_A$, with toroidal angle $\phi = \pi$. This example has $I/I_0 = 2$, and $\gamma\tau_w \approx 15$.

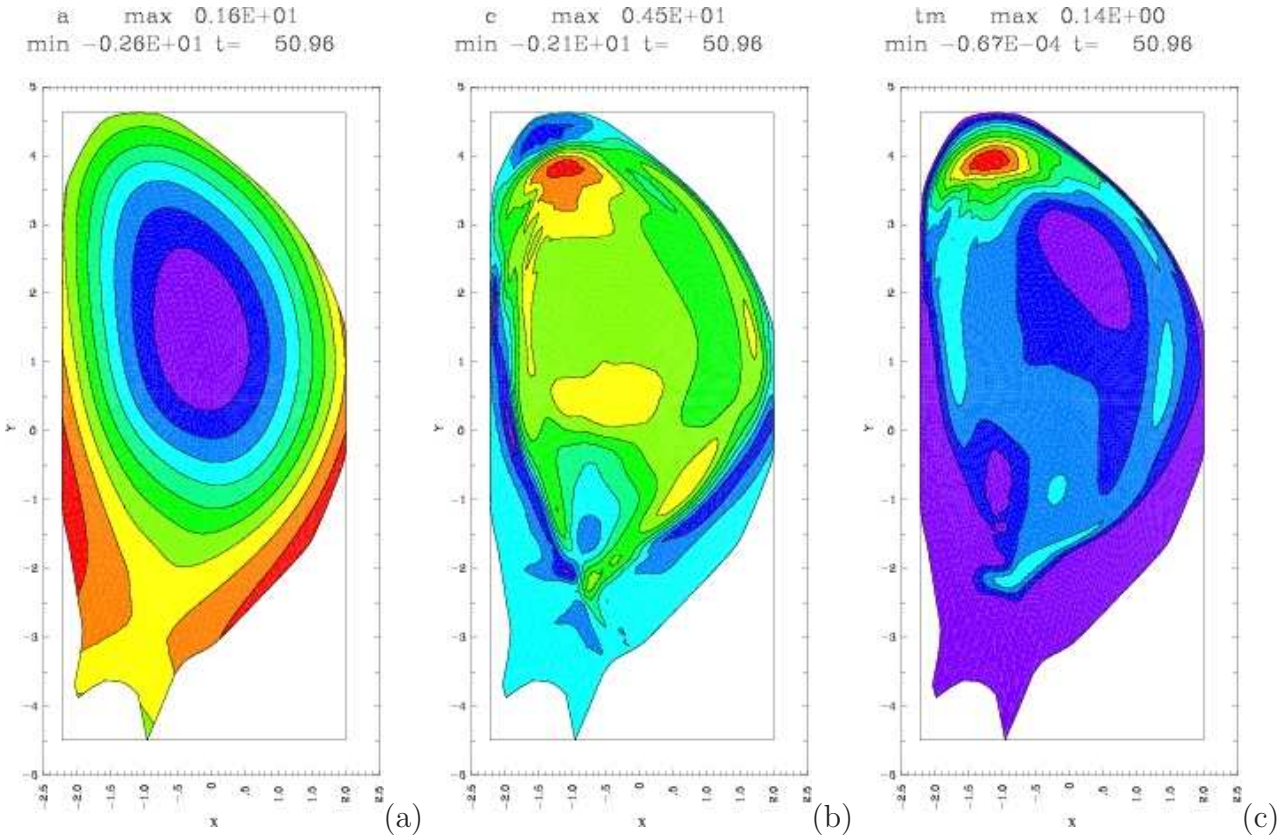

Figure 2: (a) poloidal flux ψ, (b) toroidal current $-RJ_\phi$, (c) temperature T, at $t = 51\tau_A$, with toroidal angle $\phi = \pi$.

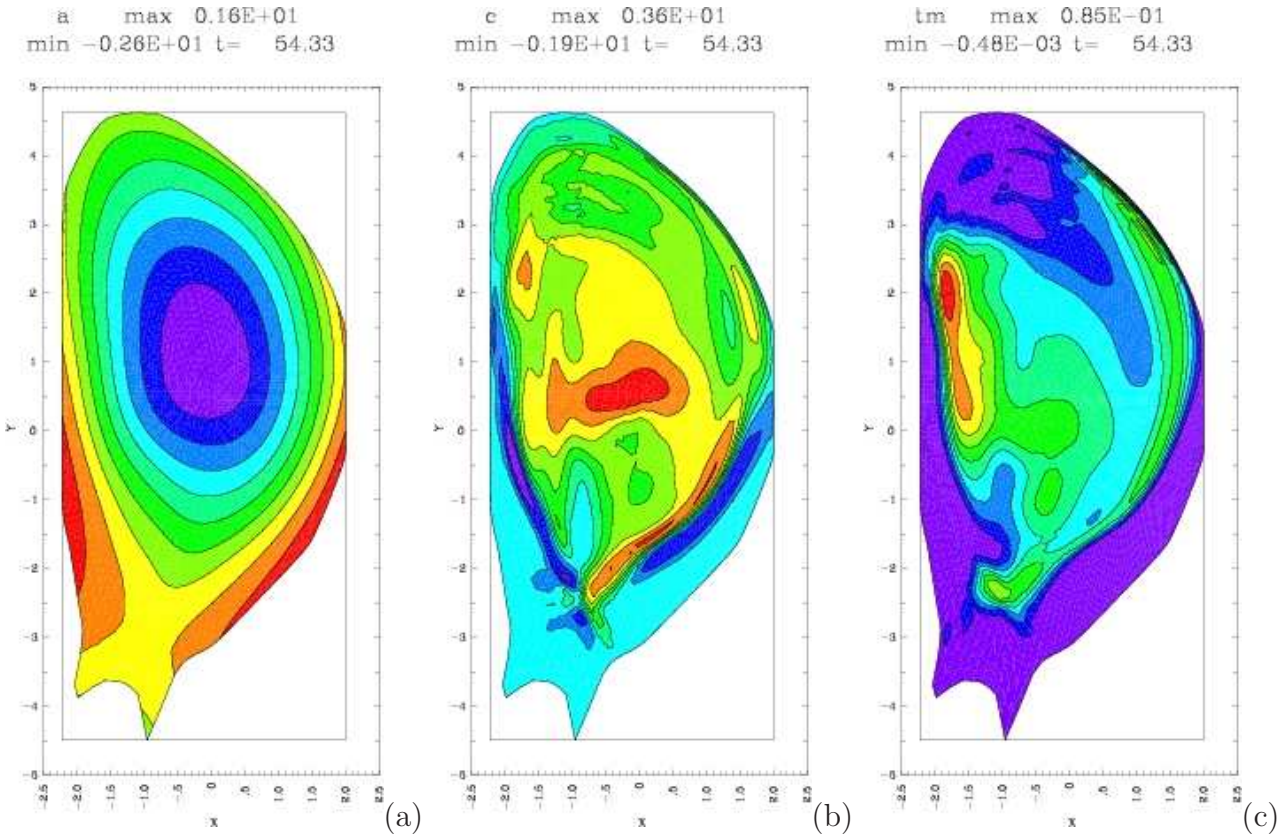

Figure 3: (a) poloidal flux ψ, (b) toroidal current $-RJ_\phi$, (c) temperature T, at $t = 54.3\tau_A$, with toroidal angle $\phi = \pi$. Current sheet, current and temperature maxima penetrate the wall.

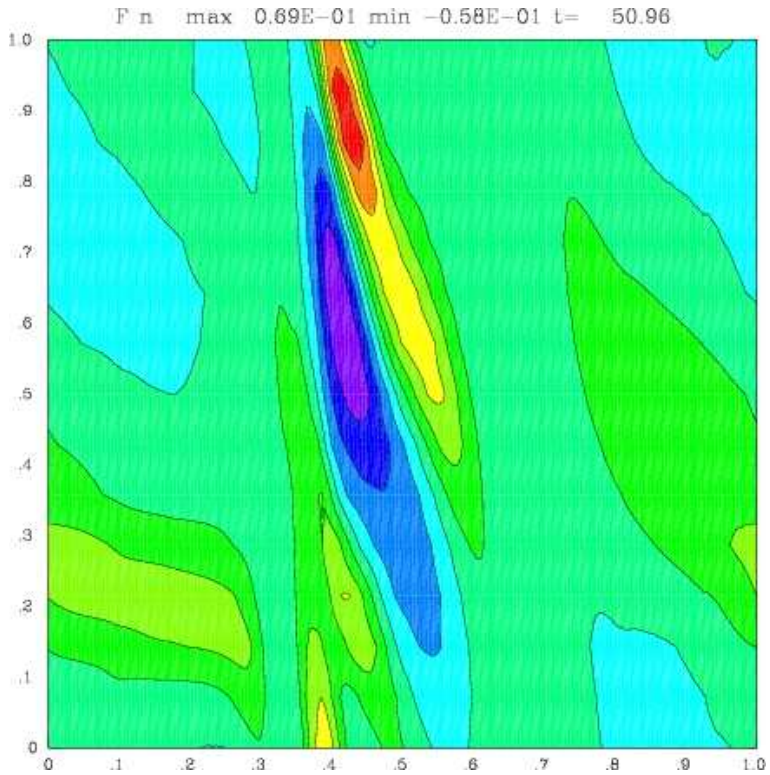

Figure 4: normal force density at $t = 51\tau_A$, $f_n(\theta, \phi)$, where θ, the poloidal angle from the origin, is the horizontal axis.

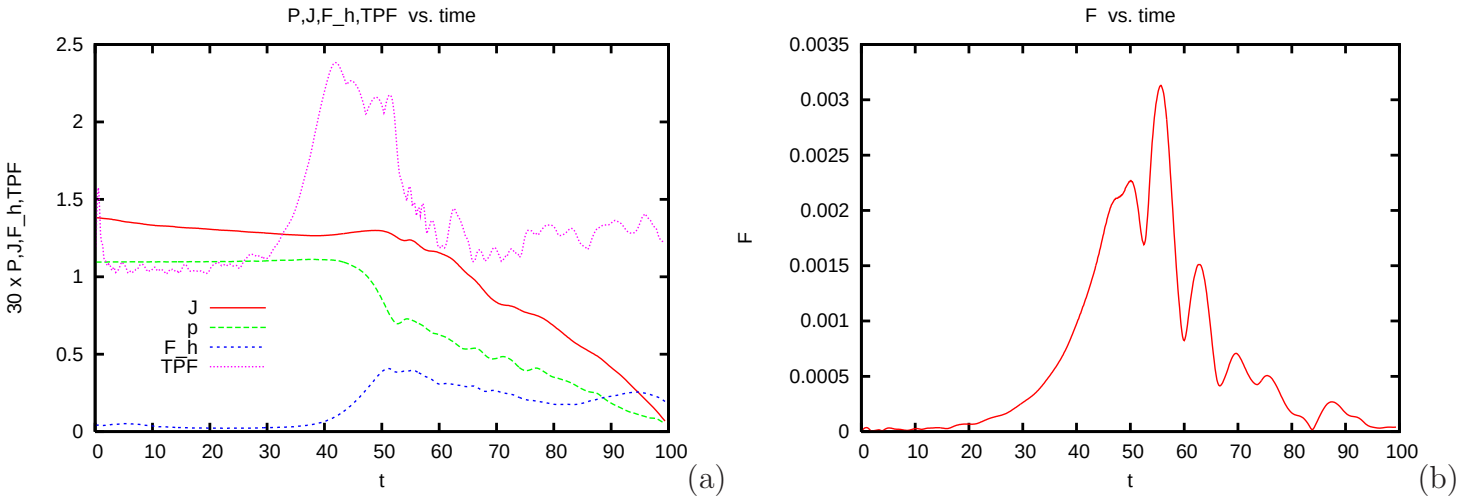

Figure 5: (a) toroidal current C, pressure p, TPF, and halo current fraction F_h as a function of time. (b) Horizontal force F_x as a function of time.

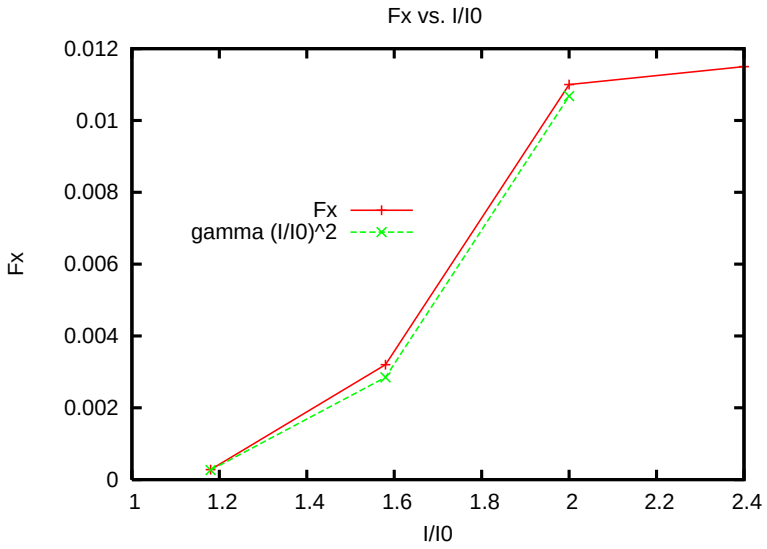

Figure 6: Scaling of wall averaged non axisymmetric horizontal force density with total current I/I_0. Also shown is $0.006\gamma(I/I_0)^2$. This scaling fits for $I/I_0 \leq 2$.

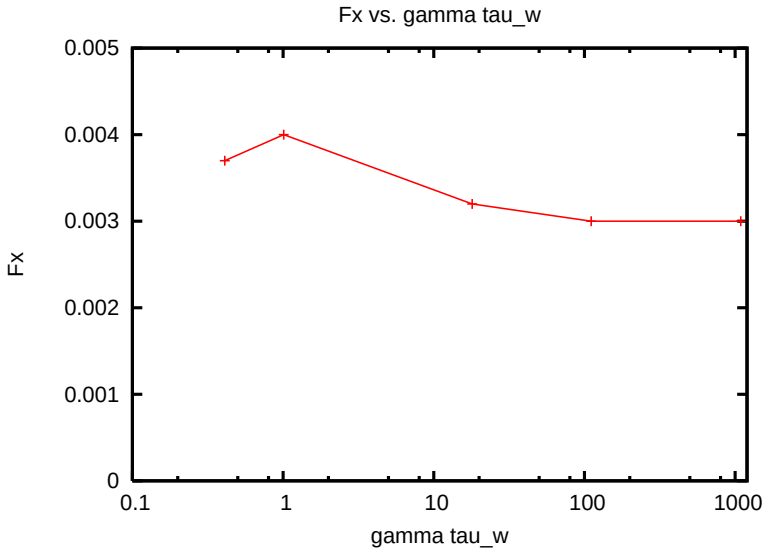

Figure 7: Scaling of horizontal F_x, with $\gamma\tau_w$. The cases shown have $I/I_0 = 1.6$. The force tends to a limit for an ideal conducting wall $\gamma\tau_w \to \infty$. The force increases for small $\gamma\tau_w$.

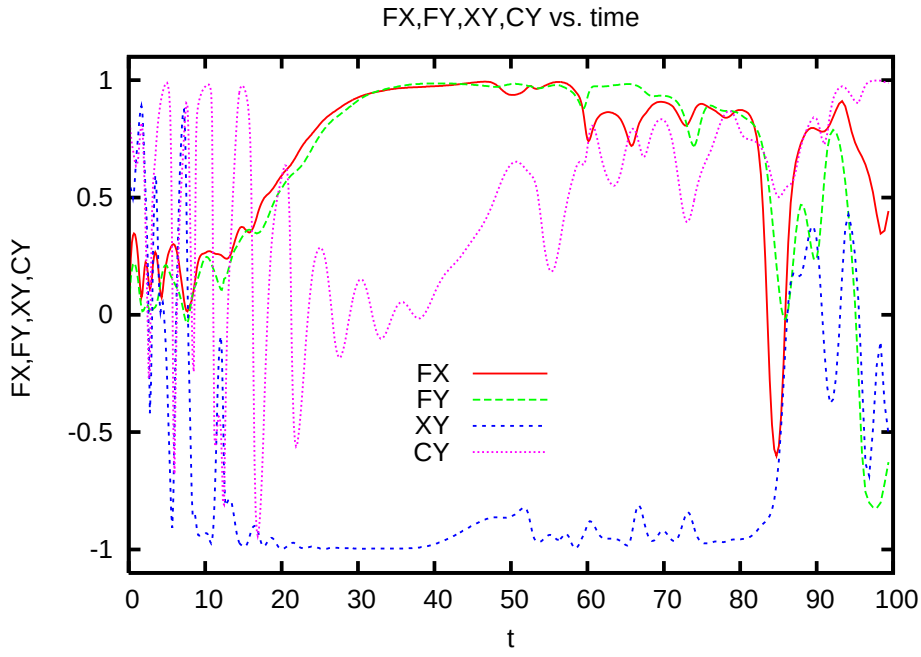

Figure 8: Correlations as a function of time. The correlations change sign after F_x is quenched.

References

[1] W. Park, E.V. Belova, G.Y. Fu, X. Tang, H.R. Strauss, L.E. Sugiyama, Plasma Simulation Studies using Multilevel Physics Models, Phys. Plasmas **6**, (1999) 1796.

[2] T. Hender *et al.* MHD stability, operational limits, and disruptions (chapter 3) Nuclear Fusion **47** S128 - 202 (2007).

[3] P.C. de Vries, M.F. Johnson, I. Segui and JET EFDA Contributors, Nucl. Fusion (2009) **49** 055011.

[4] V. Riccardo, T. C. Hender, P. J. Lomas, B. Alper, T. Bolzonella, P. de Vries, G. P. Maddison and the JET EFDA Contributors, Analysis of JET Halo Currents, Plasma Phys. Control. Fusion (2004) **46** 925

[5] V. Riccardo, P. Noll. S. P. Walker, Forces between plasma, vessel, and TF coils during AVDEs at JET, Nucl. Fusion (2000) **40** 1805.

[6] Leonid E. Zakharov, The theory of the kink mode during the vertical plasma disruption events in tokamaks, Phys. Plasmas (2008) **15** 062507.

[7] R. Paccagnella, H. R. Strauss, and J. Breslau, 3D MHD VDE and disruptions simulation of tokamak plasmas including some ITER scenarios, Nucl. Fusion (2009) **49** 035003.

[8] H. Strauss, "MHD Simulations with Resistive Wall and Magnetic Separatrix," Computer Physics Communications 164, 40 (2004).

[9] Pletzer, A., "Python & Finite Elements", Dr. Dobb's Journal #334, p. 36 (March 2002) http://ellipt2d.sourceforge.net

http://w3.pppl.gov/rib/repositories/NTCC/catalog/Asset/grin.html

[10] Chance, M., Phys. Plasmas **4**, 2161 (1997).

[11] R. B. White, D. A. Monticello, and M. N. Rosenbluth, Simulation of large magnetic islands: a possible mechanism for a major tokamak disruption, Phys. Rev. Lett. **39**, 1618 (1977)

[12] H. R. Strauss, Nonlinear three-dimensional dynamics of noncircular tokamaks, Phys. Fluids **19**, 134 (1976).

[13] B. V. Waddell, M. N. Rosenbluth, D. A. Monticello, and R. B. White, Nuclear Fusion (1977). and D. K. Lee, Phys. Rev. Lett. **41**, 1386 (1978)

[14] H.R. Strauss, Linjin Zheng, M. Kotschenreuther, W. Park, S. Jardin, J. Breslau, A. Pletzer, Roberto Paccagnella, L. Sugiyama, M. Chu, M. Chance, A. Turnbull, Halo Current and Resistive Wall Simulations of ITER, Twentieth IAEA Fusion Energy Conference, Villamora, Portugal IAEA-CN-116/TH/2-2 (2004).

[15] Pomphrey, N., Bialek, J., Park, W., "Modeling the toroidal asymmetry of poloidal halo currents," Nuclear Fusion 38, 449 (1998).

[16] A. Jameson, Analysis and Design of Numerical Schemes for Gas Dynamics 1: Artificial Diffusion, Upwind Biasing, Limiters and Their Effect Effect on Accuracy and Multigrid Convergence, International Journal of Computational Fluid Dynamics, Vol. 4 (1995) pp. 171-218.

[17] S. Orszag, On the elimination of aliasing in finite difference schemes by filtering high - wavenumber components, (1971) J. Atmos. Sci **28**. 1074.

[18] W. Park , D. Monticello, H. Strauss, J. Manickam, Phys. Fluids **2**9 (1986) 1171.

[19] H. R. Strauss and W. Longcope, An Adaptive Finite Element Method for Magnetohydrodynamics, J. Comput. Phys. 147, 318 - 336 (1998).

[20] L.L. Lao, H. St. Johh, R.D. Stambaugh, *et al.*, Nucl. Fusion **25** (1985) 1611.